Available online at www.sciencedirect.com
ScienceDirect
Journal of the European Ceramic Society 29 (2009) 2581–2588
www.elsevier.com/locate/jeurceramsoc

Microstructural changes in $(K_{0.5}Na_{0.5})NbO_3$ ceramics sintered in various atmospheres

John G. Fisher, Suk-Joong L. Kang *

Materials Interface Laboratory, Department of Materials Science and Engineering, Korea Advanced Institute of Science and Technology, 335 Gwahangno, Yusong-gu, Daejon 305-701, Republic of Korea

Received 2 December 2008; received in revised form 12 February 2009; accepted 18 February 2009
Available online 17 March 2009

Abstract

$(K_{0.5}Na_{0.5})NbO_3$ is a potential lead-free piezoelectric ceramic, but often suffers from abnormal grain growth. Previous work on $BaTiO_3$ and $SrTiO_3$ has shown that abnormal grain growth can be suppressed by controlling the sintering atmosphere. In the present work, $(K_{0.5}Na_{0.5})NbO_3$ was sintered in atmospheres ranging from O_2 to H_2 and the effect on grain growth behaviour studied. Sintering in reducing atmospheres causes a delay in the onset and a reduction in the amount of abnormal grain growth. The effect of sintering atmosphere on grain growth behaviour can be explained using the 2D nucleation-controlled theory of grain growth. Changes in the grain shape during sintering in reducing atmospheres indicate a reduction in the edge free energy of $(K_{0.5}Na_{0.5})NbO_3$ caused by an increase in the concentration of oxygen vacancies. This decreases the critical driving force necessary for rapid grain growth and causes a transition from abnormal to pseudo-normal followed by abnormal grain growth.

Keywords: Grain growth; Microstructure-final; Interfaces; Niobates; Lead-free piezoelectric

1. Introduction

A great deal of effort has gone into finding lead-free replacements for $Pb(Zr,Ti)O_3$ piezoceramics. One promising family of ceramics is based on solid solutions in the $KNbO_3$–$NaNbO_3$ pseudo-binary system.[1] Ceramics of the composition $(K_{0.5}Na_{0.5})NbO_3$ (KNN) have moderate piezoelectric properties.[2,3] The properties can be improved by addition of compounds which form a morphotropic phase boundary with KNN[4,5] and many studies have been carried out in which different compounds or additives were added to KNN. However, in spite of its importance in optimizing properties, few studies have been carried out on the grain growth behaviour of KNN.

Grain growth behaviour is strongly dependent on the structure of the grain boundaries. There are two types of grain boundary–atomically disordered (rough) and atomically ordered (faceted). Normal grain growth takes place when the grain boundaries are rough whereas abnormal grain growth can take place when the grain boundaries are faceted.[6,7] KNN has a cubic grain morphology with faceted grain boundaries[3,8] and as a consequence is prone to abnormal grain growth.[8–10] This is generally undesirable as it can impede densification and may lead to unfavourable dielectric and mechanical properties.[9,11] In $SrTiO_3$ and $BaTiO_3$, the grain boundary structure and grain growth behaviour could be controlled by varying the sintering atmosphere from oxidizing to reducing.[6,12,13] In the present work, the grain growth behaviour of KNN ceramics sintered in various atmospheres is investigated, and the results discussed in terms of the 2D nucleation-controlled theory of grain growth.

2. Experimental

The mixed oxide method was used to prepare powders of KNN.[3] $C_4H_4KNaO_6{\cdot}4H_2O$ (Fluka, 99.5%) and Nb_2O_5 (Grand Chemical & Material, 99.9%) were mixed in appropriate amounts and ball-milled in ethanol for 24 h, using ZrO_2 milling media and polypropylene jars. The Nb_2O_5 powder was dried at 250 °C overnight before weighing to remove any adsorbed water. After ball-milling the ethanol was evaporated using a hot plate and magnetic stirrer. The resulting powder was ground in an agate mortar and pestle and passed through a 180-μm sieve. The powder was loaded into an alumina crucible with lid

* Corresponding author. Tel.: +82 42 350 4113 fax: +82 42 350 8920.
E-mail address: sjkang@kaist.ac.kr (S.-J.L. Kang).

0955-2219/$ – see front matter © 2009 Elsevier Ltd. All rights reserved.
doi:10.1016/j.jeurceramsoc.2009.02.006

and calcined in air at 800 °C for 5 h. The calcined powder was examined by X-ray diffraction (Rigaku D/MAX-IIIC, Tokyo, Japan) and found to be single phase perovskite. The calcined powder was ball-milled and sieved as before to break up any agglomerates. The particle size distribution after ball-milling was measured using a laser particle size analyzer (Photal Otsuka Electronics ELS-Z2, Hirakata, Japan). The size distribution had an asymmetric single peak with a maximum at 0.11 μm and a tail out to 0.5 μm particle radius. The mean particle radius and standard deviation was 0.14 ± 0.03 μm.

Samples were made by compressing by hand 0.5 g of powder in a steel die 9 mm in diameter. Samples were then removed from the die and cold isostatically pressed at 200 MPa. Samples were sintered in atmospheres of flowing O_2, N_2, 75 N_2–25 H_2 (mol%) and H_2 (flow rate = 150 $cm^3\ min^{-1}$) at 1100 °C for periods of 1–5 h. Heating and cooling rates were 5 °C min^{-1}. To reduce volatilization of the alkali elements, the samples were placed in Pt crucibles with lids and packed in KNN powder in an alumina crucible with lid. For the samples sintered in 75 N_2–25 H_2 (mol%) and H_2, the samples were buried in the KNN powder without Pt crucibles, due to the chemical instability of Pt in reducing atmospheres. Sample masses were measured before and after sintering. Sample mass decreased by between 0.5 and 0.7% during sintering, with no dependence on sintering time or atmosphere.

Sintered samples were sectioned vertically with a diamond wheel saw, polished to a 0.25 μm finish with diamond paste and thermally etched at 1050 °C for 60 min in air. Scanning electron microscopy (SEM) was carried out using a Phillips XL30 SEM (Phillips, Eindhoven, Netherlands) with an attached Energy Dispersive Spectrometer (EDS, Model 6636, Oxford Instruments, Eynsham, UK) with standard-less quantification and LINK ISIS software. All samples were Pt coated. Grain size distributions were measured from the micrographs using an image analysis program (Matrox Inspector 2.1, Matrox Electronic Systems Ltd., Dorval, Canada). For each sample, at least 400 grains were measured. The equivalent spherical two-dimensional grain radii were measured and converted to equivalent spherical three-dimensional grain radii by dividing by 0.76.[14] For Transmission Electron Microscopy (TEM), samples were prepared by the normal methods of sectioning, dimpling and ion beam milling. Samples were viewed in a JEOL 3010 TEM (JEOL, Tokyo, Japan) with an accelerating voltage of 300 kV.

3. Results

SEM secondary electron images of ceramics sintered at 1100 °C for 1 h in different atmospheres are shown in Fig. 1. The samples sintered in O_2 and N_2 consist of coarse grains up to 10 μm in radius (Fig. 1a and b). The grains are cubic in appearance with faceted edges. Porosity is present in some of the grains. Large pores are present between the grains in both samples. Some grain pull out may also have occurred during polishing. The sample sintered in 75 N_2–25 H_2 (mol%) (Fig. 1c) has a bimodal microstructure, consisting of small matrix grains ~0.5 μm in radius and large abnormal grains up to 10 μm in

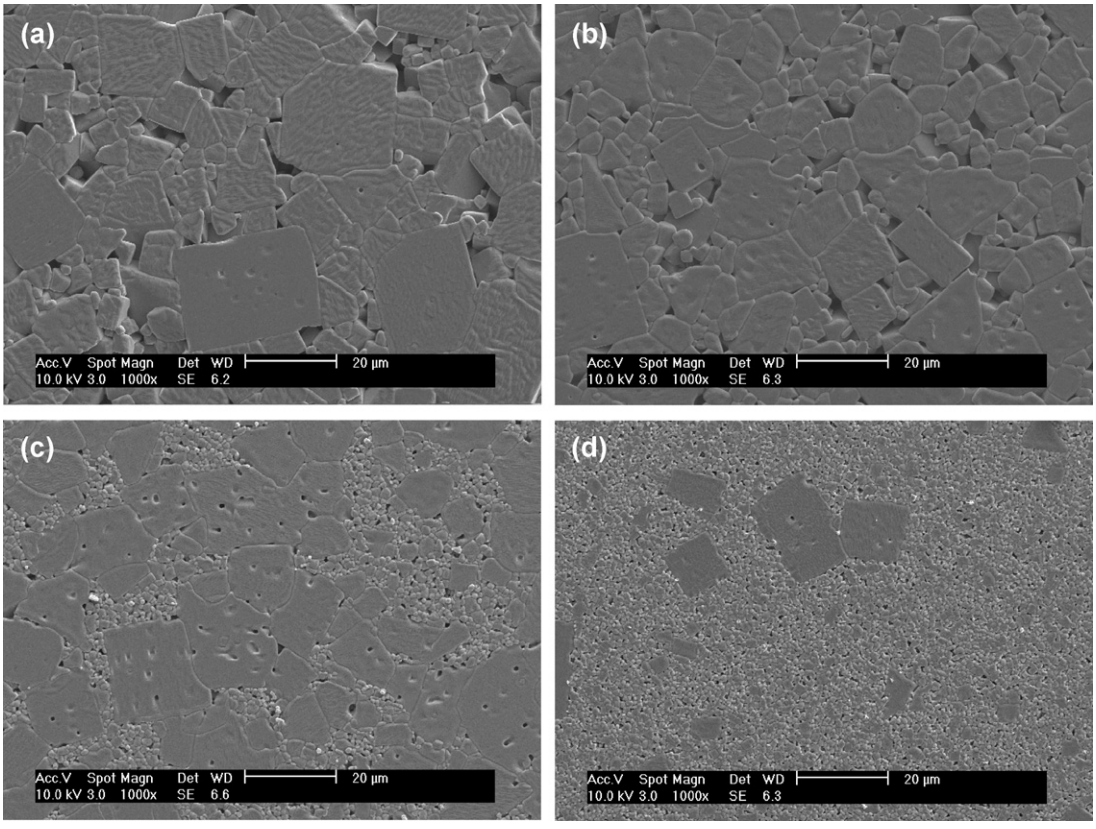

Fig. 1. SEM secondary electron images of KNN ceramics sintered at 1100 °C for 1 h in: (a) O_2; (b) N_2; (c) 75 N_2–25 H_2 (mol%) and (d) H_2.

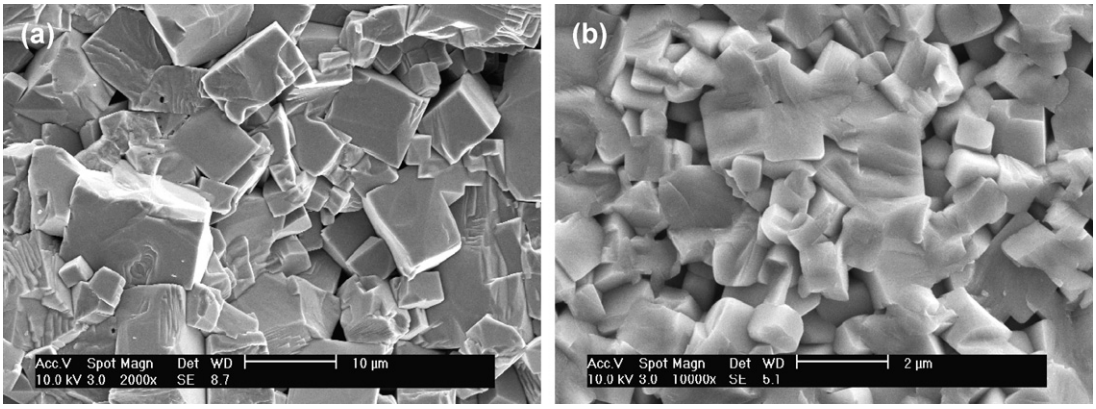

Fig. 2. SEM secondary electron images of fracture surfaces of KNN ceramics sintered at 1100 °C for 1 h in: (a) O_2 and (b) H_2.

radius. The sample sintered in H_2 (Fig. 1d) also has a bimodal microstructure, but the matrix grain size is smaller and the number of abnormal grains is greatly reduced. In the samples sintered in 75 N_2–25 H_2 (mol%) and H_2, both intragranular and intergranular porosity is present.

In the samples sintered in O_2 and N_2 for 5 h, small amounts of a second phase are visible at some of the grain boundaries. EDS of this phase shows it to be alkali deficient compared to stoichiometric KNN. In the samples sintered in 75 N_2–25 H_2 (mol%), no second phase is visible. In the samples sintered in H_2 for 3 and 5 h, small amounts of a second phase are visible but they are too small to carry out EDS on.

Fracture surfaces of samples sintered at 1100 °C for 1 h in O_2 and H_2 are shown in Fig. 2. The sample sintered in O_2 consists of cube-shaped grains with sharp edges and corners (Fig. 2a). The sample sintered in H_2 also consists of cubic grains but some of the edges and corners are rounded (Fig. 2b).

The grain size distributions for the samples sintered in O_2 are shown in Fig. 3. The grain size distributions are fitted with two Gaussian curves (the dashed lines are the individual curves and the solid line is the combined curve). The grains that lie within the first peak can be considered to be the normal matrix grains. The mean matrix grain radius $\bar{r}$ of the first peak is given next to each distribution. The grains that lie outside the first peak of each combined curve are abnormal grains. After 1 h, the grain size distribution of the sample sintered in O_2 is already abnormal, with several distinct peaks. As the sintering time increases, grain growth continues and the grain size distribution shifts to larger sizes. The distribution becomes more unimodal, but very broad. The grain size distributions of the samples sintered in N_2 follow the same pattern, but are slightly narrower.

The grain size distributions of the samples sintered in 75 N_2–25 H_2 (mol%) are shown in Fig. 4. A single Gaussian curve is plotted for each grain size distribution (the solid lines). The mean matrix grain radius $\bar{r}$ of this curve is given next to each distribution. The abnormal grains lie outside the curve. The largest abnormal grain in each distribution is marked with an arrow.

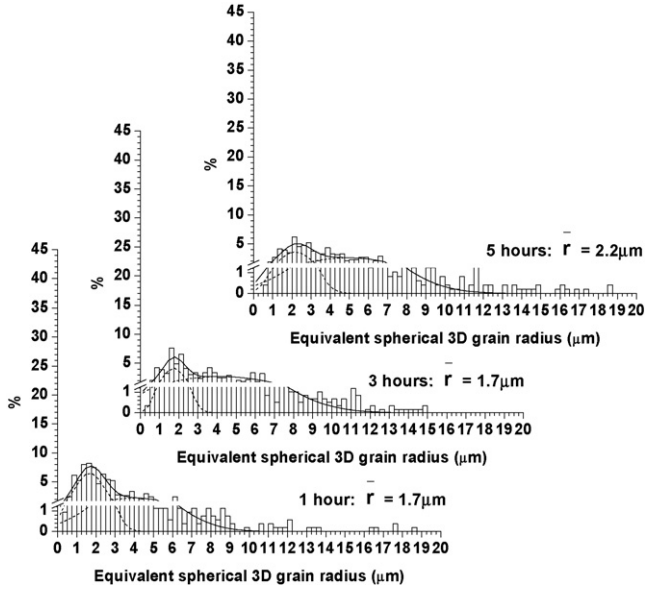

Fig. 3. Grain size distributions of KNN ceramics sintered at 1100 °C for 1, 3 and 5 h in O_2. $\bar{r}$ = mean matrix grain radius.

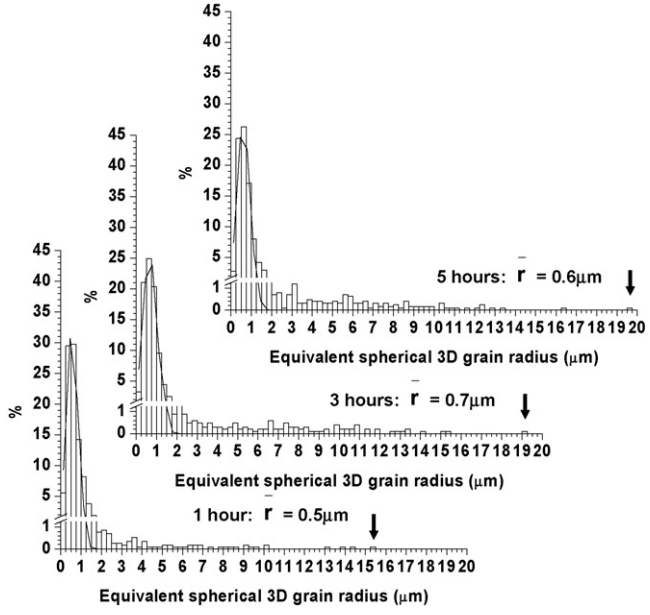

Fig. 4. Grain size distributions of KNN ceramics sintered at 1100 °C for 1, 3 and 5 h in 75 N_2–25 H_2 (mol%). $\bar{r}$ = mean matrix grain radius.

The grain size distribution of the sample sintered for 1 h is much narrower than that of the equivalent sample sintered in O_2, but is still bimodal. As sintering continues, the main peak becomes broader and the number and size of abnormal grains increases. After 3 h, grain growth in the main peak stops, but the abnormal grains continue to grow.

The grain size distributions of the samples sintered in H_2 are shown in Fig. 5. Again, a single Gaussian curve is plotted for each grain size distribution (the solid lines), with the abnormal grains lying outside the curve. The mean matrix grain radius $\bar{r}$ of this curve is given next to each distribution. The largest abnormal grain in each distribution is marked with an arrow. Compared to the sample sintered in 75 N_2–25 H_2 (mol%), the sample sintered in H_2 for 1 h has a slightly narrower grain size distribution and a smaller number of abnormal grains. As the sintering time increases, the main peak begins to broaden and more abnormal grains appear. The number and size of abnormal grains are reduced compared to the samples sintered in 75 N_2–25 H_2 (mol%). Again, after 3 h, grain growth in the main peak stops. The abnormal grains continue to grow, but at a slower rate compared to the samples sintered in 75 N_2–25 H_2 (mol%).

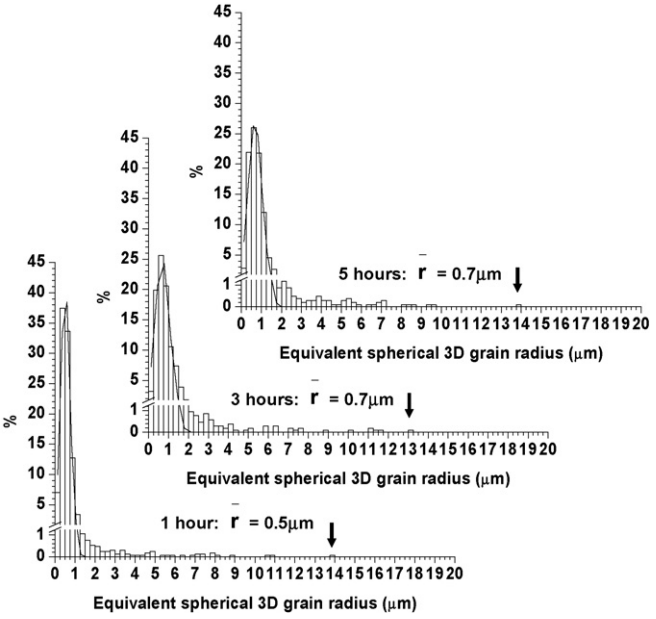

Fig. 5. Grain size distributions of KNN ceramics sintered at 1100 °C for 1, 3 and 5 h in H_2. $\bar{r}$ = mean matrix grain radius.

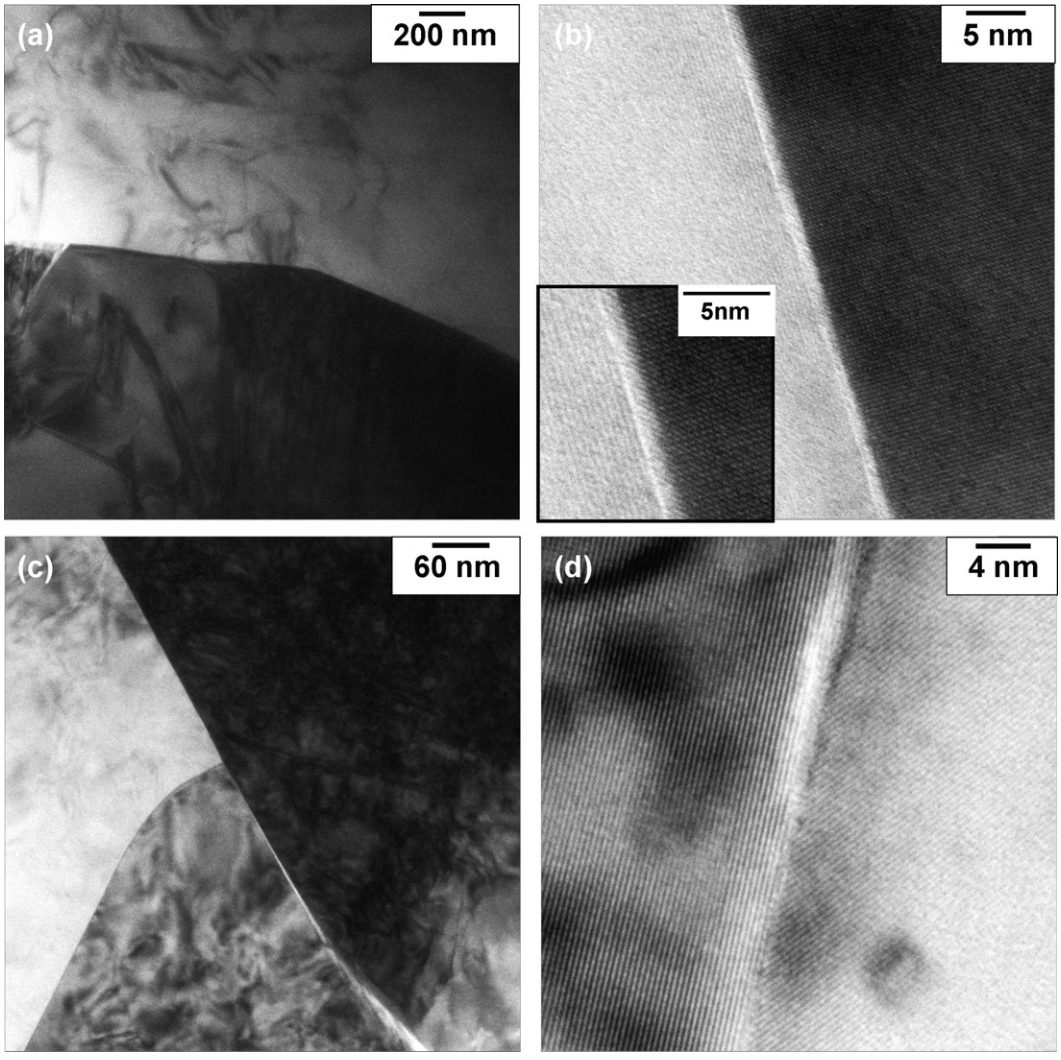

Fig. 6. TEM images of KNN ceramics sintered at 1100 °C for 1 h in O_2 [(a) and (b)] and H_2 [(c) and (d)].

TEM micrographs of the sample sintered in O_2 for 1 h are shown in Fig. 6. The sample has faceted grain boundaries (Fig. 6a). No secondary phases are visible at the grain boundaries or triple junctions. A high-resolution image of a typical grain boundary is shown in Fig. 6b. The grain boundary is atomically faceted. The inset in Fig. 6b is an enlarged portion of the image and shows that the grain boundary is free of amorphous phase. The triple junctions are also free of amorphous phase. TEM micrographs of the sample sintered in H_2 for 1 h are also shown in Fig. 6. Some of the grain boundaries in this sample are faceted while others are curved at the triple junctions (Fig. 6c). No secondary phases are visible. High-resolution imaging of the grain boundaries again reveals faceting on an atomic scale and no amorphous phase (Fig. 6d). Again, no amorphous phase is visible at the triple junctions.

4. Discussion

All of the KNN samples show abnormal grain growth (Fig. 1). Normal grain growth is characterized by a unimodal grain size distribution, whereas abnormal grain growth is characterized by a very broad, bimodal or even multimodal grain size distribution.[7] Broad multimodal grain size distributions can be seen for the samples sintered in O_2 and N_2 (Fig. 3). As the sintering atmosphere becomes more reducing, abnormal grain growth is impeded. The main peak of the grain size distributions becomes narrower and the number of abnormal grains decreases (Figs. 4 and 5), although abnormal grain growth is not entirely eliminated.

The atomic structure of the grain boundaries (rough or faceted) plays an important role in controlling the grain growth behaviour.[6,7,12,13] The influence of grain boundary structure on grain growth can be explained using theories of crystal growth. Although originally used to describe crystal growth from solution, there is evidence that solid-state grain boundaries can behave in the same fashion.[15–17] The variation of grain growth rate with driving force for grain growth is shown schematically in Fig. 7. In a system with atomically rough grain boundaries, atoms can attach to any site on a growing grain.[18] Grain growth is controlled by the rate of atomic diffusion across the grain boundary and the grain growth rate increases linearly with the driving force for grain growth (the dashed line in Fig. 7). In such a system, any grain with a positive driving force can grow and normal grain growth is observed.

In a system with atomically faceted grain boundaries, atoms cannot attach to a grain unless a low energy site such as a 2D nucleus is present.[18] Consequently, grain growth is limited by the rate at which stable 2D nuclei can form on the grain surface. Below a critical driving force ΔG_C, the rate at which stable 2D nuclei form is very low. Atoms adsorbing on the surface of the grain will have a low probability of reaching a 2D nucleus before they desorb again and the grain growth rate will be negligibly slow. Above the critical driving force, the rate at which stable 2D nuclei form increases rapidly. Atoms adsorbing on the grain have a high probability of reaching a 2D nucleus and grain growth will be rapid. Grain growth is then effectively controlled by diffusion, as in the case of grains with atomically rough boundaries. When

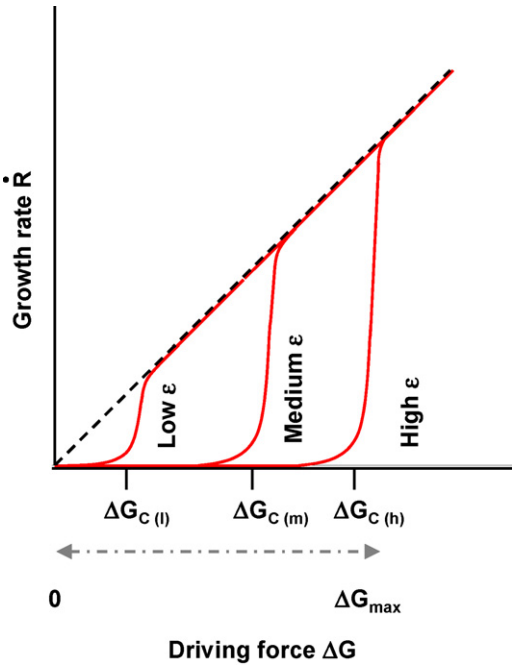

Fig. 7. Grain growth rate vs. driving force for growth for diffusion (dotted line) and 2D nucleation-controlled growth (solid lines).

the driving force is approximately equal to the critical driving force, grain growth will take place but the growth rate will be low. The growth rate of a faceted grain does not increase linearly with the driving force for grain growth but exponentially (the solid lines in Fig. 7). For a grain growing by 2D nucleation-controlled growth, the growth rate can be given by[19]:

$$\dot{R} \cong \upsilon_{st} \exp\left(\frac{-\pi\Omega\varepsilon^2}{6\Delta G h k T}\right) \quad (1)$$

where $\dot{R}$ = growth rate, υ_{st} = step velocity of the growing nucleus, Ω = molar volume, ε = edge free energy of the nucleus, ΔG = driving force for grain growth, h = step height of the nucleus, k = Boltzman's constant and T = temperature. For the case of a grain growing in the solid-state, the driving force is given by[20]:

$$\Delta G = \sigma_{gb}\Omega\left(\frac{1}{\bar{r}} - \frac{1}{r}\right) \quad (2)$$

where σ_{gb} is the average grain boundary energy, r is the radius of the growing grain and $\bar{r}$ is the radius of a grain which is neither growing nor shrinking (usually given by the mean grain radius). The driving force of a grain is inversely related to the mean grain radius. The critical driving force is given by[19]:

$$\Delta G_C = \frac{\Omega\varepsilon^2}{3hkT} \quad (3)$$

The grains will have a range of driving forces for growth, depending on their radii (shown by the dash–dotted arrow in Fig. 7). This range of driving forces is initially determined by the particle size distribution of the starting powder. For a system where grain growth is controlled by 2D nucleation, the grains may be categorized into three types: dissolving grains (ΔG is

negative), grains with non-linear growth rates governed by interface reaction, which include stagnant, i.e., non-growing grains ($0 < \Delta G < \Delta G_C$) and slowly growing grains ($\Delta G \approx \Delta G_C$), and rapidly growing grains with linear growth rates governed by diffusion ($\Delta G > \Delta G_C$). The largest grain will have the largest driving force for growth ΔG_{max}.

Depending on the relative values of ΔG_C and ΔG_{max}, different types of grain growth behaviour can take place.[12,21–24] If $\Delta G_C \gg \Delta G_{max}$, no grains will have $\Delta G > \Delta G_C$ and grain growth rates will be negligibly slow, i.e., stagnant grain growth occurs. If $\Delta G_C \leq \Delta G_{max}$, then most grains will be growing slowly or not at all, but a small number of grains will have $\Delta G > \Delta G_C$ and will be able to grow rapidly to form abnormal grains. Because the majority of grains are not growing or are growing slowly, the mean grain radius $\bar{r}$ remains small. The driving force for growth of the abnormal grains will remain high and they will continue to grow until all the matrix grains are consumed. At this point, $\bar{r}$ will increase abruptly, ΔG will decrease and grain growth will slow down. If $\Delta G_C \ll \Delta G_{max}$, a large number of grains have $\Delta G > \Delta G_C$ and are able to grow. Pseudo-normal grain growth takes place. The grain size distribution will initially be unimodal but abnormal grains may develop after extended sintering. Finally, if ΔG_C equals zero, then all grains with a positive driving force can grow and normal diffusion-controlled grain growth takes place.[22,23,24]

From Eq. (3), it can be seen that the value of ΔG_C is strongly dependent on the edge free energy ε of the 2D nucleus. The step energy of steps on a vicinal surface, which is analogous to ε, is inversely related to the configurational entropy.[25–27] The configurational entropy can be increased by the formation of kinks in a step due to thermal excitation[27] or by the creation of vacancies.[28] Therefore, a change in the vacancy concentration can change the value of ε and affect the grain growth behaviour. In experiments carried out on $BaTiO_3$ and $SrTiO_3$, increasing the vacancy concentration (by donor doping or sintering in reducing atmospheres) caused a decrease in ε sufficient to change the grain boundaries from faceted to rough. This in turn caused the grain growth behaviour to change from abnormal to normal.[6,12,13]

XRD, Differential Scanning Calorimetry and Raman spectroscopy carried out on KNN samples sintered in reducing atmospheres indicate a reduction in the orthorhombic distortion of the KNN unit cell, a lowering of the phase transition temperatures and an increase in the Nb–O bond length.[29] These changes can be attributed to an increase in the oxygen vacancy concentration, which would be expected to decrease ε. Indeed, the rounding of the grain corners and edges of the samples sintered in H_2 indicates a decrease in ε and partial roughening of the grain boundaries as the sintering atmosphere becomes more reducing (Figs. 2b and 6c).[30–33] Therefore, the grain growth behaviour of KNN in different atmospheres can be explained by considering the change in ε and ΔG_C.

The KNN samples sintered in O_2 have faceted grain boundaries (Figs. 1a, 2a and 6a). This indicates a high value of ε and, correspondingly, ΔG_C ($\Delta G_{C\,(h)}$ in Fig. 7).[31–33] In the samples sintered in O_2 and N_2, the microstructure is coarse with many abnormal grains (Fig. 1a and b) and the grain size distributions are broad with a main peak and several minor peaks (Fig. 3). This microstructure is consistent with a system where $\Delta G_C \leq \Delta G_{max}$, as mentioned above. The small number of grains with $\Delta G > \Delta G_C$ will be able to grow rapidly to form abnormal grains as they have a high growth rate. After sintering for 1 h, the process of abnormal grain growth is well advanced and almost all of the original matrix grains have already been consumed by abnormal grains. The grain growth rate decreases as sintering continues and the grain size distribution becomes more unimodal, due to impingement of abnormal grains.

In the samples sintered in 75 N_2–25 H_2 (mol%), the vacancy concentration increases and ε decreases. A decrease in ε will cause a decrease in ΔG_C ($\Delta G_{C\,(m)}$ in Fig. 7) while ΔG_{max} remains unchanged. In this case, $\Delta G_C \ll \Delta G_{max}$, a large number of grains can grow and pseudo-normal grain growth occurs. In the initial stage of sintering, there is not a large difference in the growth rates between the growing grains. Grains with driving forces close to ΔG_{max} do not enjoy a significant growth advantage over other growing grains and so abnormal grains do not form. As sintering proceeds, the mean grain size $\bar{r}$ will increase, leading to a reduction in the driving force for each grain (Eq. (2)), a reduction in ΔG_{max} and a decrease in the number of grains with $\Delta G > \Delta G_{C\,(m)}$. As the driving force of a grain becomes approximately equal to $\Delta G_{C\,(m)}$, its growth rate will decrease considerably. Once the growth rate of the majority of grains has decreased, grains which still have $\Delta G > \Delta G_{C\,(m)}$ will now be growing at a rate much faster than grains with $\Delta G \approx \Delta G_{C\,(m)}$ and can form abnormal grains. After 1 h of sintering, the process of abnormal grain growth is under way but is not completed (Figs. 1c and 4). With increased sintering time, the abnormal grains continue to grow. The matrix grains (the grains in the main peak of the grain size distribution) are also growing slowly, which will cause their driving force for growth to decrease further. Eventually, the matrix grains will have values of $\Delta G < \Delta G_{C\,(m)}$ and matrix grain growth will stop. This happens after 3 h of sintering (Fig. 4). The growth rate of the abnormal grains will also slow down as they impinge upon each other. Such time-delayed abnormal grain growth has also recently been observed for liquid phase-sintered ceramics in the $(Na_{0.5}Bi_{0.5})TiO_3$–$BaTiO_3$ system.[34]

In the samples sintered in H_2, ΔG_C is reduced even further ($\Delta G_{C\,(l)}$ in Fig. 7) and the number of grains which are able to grow will increase. Due to the low value of $\Delta G_{C\,(l)}$, the majority of grains can grow for a longer period of time before their driving force becomes approximately equal to $\Delta G_{C\,(l)}$ and their growth rate decreases. The time that must pass before abnormal grain growth can start will therefore increase. After 1 h of sintering, abnormal grain growth has only just begun (Figs. 1d and 5). After abnormal grain growth begins, abnormal and matrix grain growth continues in parallel. Again, after 3 h of sintering all the matrix grains have values of $\Delta G < \Delta G_{C\,(l)}$ and matrix grain growth stops. The abnormal grains can continue to grow but at a relatively slow rate as their driving force for growth is now low compared to that of the samples sintered in 75 N_2–25 H_2 (mol%).

Transitions from abnormal to normal grain growth associated with roughening of the grain corners and edges have also been observed in liquid phase-sintered systems such as

NbC-Co[31] and $Pb(Mg_{1/3}Nb_{2/3})O_3$–$PbTiO_3$ with excess PbO.[35] From the present work, KNN appears to behave in a similar manner to $Pb(Mg_{1/3}Nb_{2/3})O_3$–$PbTiO_3$, where the transition from abnormal to normal grain growth was accompanied by a small amount of roughening at the grain corners and edges.[35]

Other factors that could affect grain growth in KNN-based ceramics include porosity and the presence of a liquid phase. The samples sintered in 75 N_2–25 H_2 (mol%) and H_2 appear more porous than the samples sintered in O_2 and N_2 (Fig. 1). Pores at the grain boundaries of the matrix grains can inhibit grain growth by pore drag.[36] If a grain has a high enough driving force to grow abnormally, its grain boundaries can break free of the pores, leaving them trapped in the grain. This can be seen in Fig. 1. By comparing the values of the mean matrix grain radius (Figs. 3–5), it can be seen that changing the sintering atmosphere from O_2 to 75 N_2–25 H_2 (mol%) causes a decrease in the matrix grain growth rate, but further changing the sintering atmosphere to H_2 has no effect. It appears that an increase in porosity affects the matrix grain growth rate. The increased porosity may reduce the driving force ΔG for grain growth due to an increase in pore drag.[36] This would reduce ΔG_{max}, which would reduce the number of grains that could grow abnormally if ΔG_C remains constant. However, ΔG_C also decreases as the sintering atmosphere becomes more reducing. The effect of increased porosity on formation and growth of abnormal grains is therefore minimized, as it is the relative values of ΔG_C and ΔG_{max} which determine whether abnormal grains are formed.

Zhen and Li, and Li et al. observed abnormal grain growth in Li/Ta-doped KNN ceramics, which they attributed to the presence of a liquid phase caused by alkali volatilization.[9,37] In the present work, it is possible that the samples sintered in O_2 or N_2 may have suffered alkali volatilization,[38,39] which could lead to the formation of a liquid phase. Small amounts of an alkali-deficient second phase were visible at some of the grain boundaries in samples sintered in O_2 and N_2 for 5 h or in H_2 for $\geq$3 h. This second phase may have been liquid at the sintering temperature.[40] However, a liquid phase is not present at the grain boundaries or triple junctions of the samples sintered for 1 h, irrespective of sintering atmosphere (Fig. 6b and d). After 1 h of sintering, the microstructure of the samples has already developed and further sintering does not produce any drastic changes. In addition, recent work on KNN and $BaTiO_3$ has shown that the presence of a liquid phase can reduce the mobility of grain boundaries.[41,42] Therefore, we consider the decrease in the edge free energy ε of samples sintered in reducing atmospheres, as shown by roughening at the grain corners and edges, to be the cause of the change in grain growth behaviour.

In the samples sintered in 75 N_2–25 H_2 (mol%) and H_2, the matrix grain size increases with sintering time up to 3 h and then stops (Figs. 4 and 5). This is expected as the driving force for grain growth decreases as $\bar{r}$ increases (Eq. (2)). However, grain growth continues in the samples sintered in O_2 and N_2 even up to 5 h (Fig. 3). This may be due to the broader grain size distribution of these samples, as in the case of $BaTiO_3$ doped with Al_2O_3.[43] In a sample with a bimodal grain distribution, $\bar{r}$ may be determined by the grains in the first peak, as these are dissolving.[44] The grains in the second peak then may have a large enough driving force to continue growing. Repeated waves of abnormal grain growth have recently been predicted in model calculations of grain growth in liquid phase-sintered systems.[22,23,24]

5. Conclusions

KNN ceramics were sintered in atmospheres ranging from O_2 to H_2. All samples display abnormal grain growth, but the amount of abnormal grain growth is reduced as the sintering atmosphere becomes more reducing. In addition, samples sintered in reducing atmospheres show a time delay in the onset of abnormal grain growth. Samples sintered in H_2 show partial roughening of the grain edges and corners. This indicates a decrease in the edge free energy of the grains caused by an increase in vacancy concentration. The decrease in edge free energy decreases the critical driving force necessary for 2D nucleation-controlled grain growth, causing the grain growth behaviour to change from abnormal to pseudo-normal followed by abnormal growth.

Acknowledgements

This work was funded by a grant from the Center for Advanced Materials Processing CAMP (21st Century Frontier R&D Program funded by the Ministry of Commerce, Industry and Energy [MOCIE], Republic of Korea, Grant No. PM007-8-01-01) and a Korea Research Foundation Grant from the Korean Government (Ministry of Education and Human Resources Development Grant KRF-2005-005-J09701). The authors would like to thank Seon Young Lee and Su Min Shin for operating the SEM and TEM, respectively.

References

1. Jaffe, B., Cook Jr., W. R. and Jaffe, H., *Piezoelectric Ceramics*. Academic Press, London, 1971, pp. 192–193.
2. Jaeger, R. E. and Egerton, L., Hot pressing of potassium-sodium niobates. *J. Am. Ceram. Soc.*, 1962, **45**(5), 209–213.
3. Malic, B., Bernard, J., Holc, J., Jenko, D. and Kosec, M., Alkaline-earth doping in (K,Na)NbO_3 based piezoceramics. *J. Eur. Ceram. Soc.*, 2005, **25**, 2707–2711.
4. Guo, Y., Kakimoto, K. and Ohsato, H., $(Na_{0.5}K_{0.5})NbO_3$–$LiTaO_3$ lead-free piezoelectric ceramics. *Mater. Lett.*, 2005, **59**, 241–244.
5. Zuo, R., Fang, X. and Ye, C., Phase transitional behavior and piezoelectric properties of lead-free $(Na_{0.5}K_{0.5})NbO_3$–$(Bi_{0.5}K_{0.5})TiO_3$ ceramics. *J. Am. Ceram. Soc.*, 2007, **90**(8), 2424–2428.
6. Chung, S. Y., Yoon, D. Y. and Kang, S.-J. L., Effects of donor concentration and oxygen partial pressure on interface morphology and grain growth behavior in $SrTiO_3$. *Acta Mater.*, 2002, **50**, 3361–3371.
7. Kang, S.-J. L., *Sintering: Densification, Grain Growth and Microstructure*. Elsevier, Amsterdam, 2005, pp. 117–124.
8. Jenko, D., Benčan, A., Malič, B., Holc, J. and Kosec, M., Electron microscopy studies of potassium sodium niobate ceramics. *Microsc. Microanal.*, 2005, **11**, 572–580.
9. Zhen, Y. and Li, J. F., Abnormal grain growth and new core–shell structure in (K,Na)NbO_3-based lead-free piezoelectric ceramics. *J. Am. Ceram. Soc.*, 2007, **90**(11), 3496–3502.
10. Malic, B., Bernard, J., Bencan, A. and Kosec, M., Influence of zirconia addition on the microstructure of $K_{0.5}Na_{0.5}NbO_3$ ceramics. *J. Eur. Ceram. Soc.*, 2008, **28**, 1191–1196.

11. Chiang, Y. M., Birnie III, D. and Kingery, W. D., *Physical Ceramics: Principles for Ceramic Science and Engineering*. John Wiley & Sons, New York, 1997, pp. 351–513.
12. Jung, Y. I., Choi, S. Y. and Kang, S.-J. L., Effect of oxygen partial pressure on grain boundary structure and grain growth behavior in $BaTiO_3$. *Acta Mater.*, 2006, **54**, 2849–2855.
13. Lee, B. K., Chung, S. Y. and Kang, S. –J. L., Grain boundary faceting and abnormal grain growth in $BaTiO_3$. *Acta Mater.*, 2000, **48**, 1575–1580.
14. Schatt, W. and Wieters, K. P., *Powder Metallurgy*. European Powder Metallurgy Association, Bellstone, Shrewsbury, UK, 1997.
15. Merkle, K. L. and Thompson, L. J., Atomic-scale observation of grain boundary motion. *Mater. Lett.*, 2001, **48**, 188–193.
16. Tsurekawa, S., Ueda, T., Ichikawa, K., Nakashima, H., Yoshitomi, Y. and Yoshinaga, H., Grain boundary migration in Fe-3% Si bicrystal. *Mat. Sci. Forum*, 1996, **204–206**, 221–226.
17. Yoon, B. K., Chung, S. Y. and Kang, S.-J. L., Nonlinear migration of faceted grain boundaries with driving force in barium titanate, to be published.
18. Hirth, J. P. and Pound, G. M., *Condensation and Evaporation: Nucleation and Growth Kinetics*. Pergamon Press, Oxford, 1963, pp. 77–101.
19. van der Eerden, J. P., Crystal growth mechanisms. In *Handbook of Crystal Growth, Vol. 1, Fundamentals, Part A, Thermodynamics and Kinetics*, ed. D. T. J. Hurle. Elsevier Science Publishers, Amsterdam, Netherlands, 1993, pp. 311–475.
20. Yoon, D. Y., Park, C. W. and Koo, J. B., The step growth hypothesis for abnormal grain growth. In *Ceramic Interfaces 2*, ed. H. I. Yoo and S.-J. L. Kang. Institute of Materials, London, 2001, pp. 3–21.
21. Fisher, J. G., Kim, M. S., Lee, H. Y. and Kang, S.-J. L., Effect of Li_2O and PbO additions on abnormal grain growth in the $Pb(Mg_{1/3}Nb_{2/3})O_3$-35 mol% $PbTiO_3$ system. *J. Am. Ceram. Soc.*, 2004, **87**(5), 937–942.
22. Kang, S.-J. L., Jung, Y. I. and Moon, K. S., Principles of microstructural design in two-phase systems. *Mat. Sci. Forum*, 2007, **558–559**, 827–854.
23. Kang, S.-J. L., Lee, M. G. and An, S. M., Microstructural evolution during sintering with control of interface structure. *J. Am. Ceram. Soc.*, in press.
24. Jung, Y. I., Yoon, D. Y. and Kang, S.-J. L., Coarsening of polyhedral grains in a liquid matrix, in press.
25. Burton, W. K., Cabrera, N. and Frank, F. C., The growth of crystals and the equilibrium structure of their surfaces. *Philos. Trans. R. Soc. Lond. Ser. A*, 1951, **243**, 299–358.
26. Williams, E. D. and Bartelt, N. C., Thermodynamics of surface morphology. *Science*, 1991, **251**, 393–400.
27. Williams, E. D., Surface steps and surface morphology: understanding macroscopic phenomena from atomic observations. *Surf. Sci.*, 1994, **299–300**, 502–524.
28. Chiang, Y. M., Birnie III, D. and Kingery, W. D., *Physical Ceramics: Principles for Ceramic Science and Engineering*. John Wiley & Sons, New York, 1997, pp. 101–184.
29. Fisher, J. G., Rout, D., Moon, K. S. and Kang, S.-J. L., Structural changes in potassium sodium niobate ceramics sintered in different atmospheres. *J. Alloys Compd.*, 2009, doi:10.1016/j.jallcom.2008.12.100.
30. Choi, S. Y. and Kang, S.-J. L., Sintering kinetics by structural transition at grain boundaries in barium titanate. *Acta Mater.*, 2004, **52**, 2937–2943.
31. Cho, Y. K., Yoon, D. Y. and Kim, B. K., Surface roughening transition and coarsening of NbC grains in liquid cobalt-rich matrix. *J. Am. Ceram. Soc.*, 2004, **87**(3), 443–484.
32. Yoon, D. Y. and Cho, Y. K., Roughening transition of grain boundaries in metals and oxides. *J. Mater. Sci.*, 2005, **40**, 861–870.
33. Jo, W., Kim, D. Y. and Hwang, N. M., Effect of interface structure on the microstructural evolution of ceramics. *J. Am. Ceram. Soc.*, 2006, **89**(8), 2369–2380.
34. Moon, K.-S. and Kang, S.-J. L., Coarsening behavior of round-edged cubic grains in the $Na_{1/2}Bi_{1/2}TiO_3$–$BaTiO_3$ system. *J. Am. Ceram. Soc.*, 2008, **91**(10), 3191–3196.
35. Seo, C. E., Yoon, D. Y., Wallace, J. S. and Blendell, J. E., Dependence of grain shape and growth on PT content in PbO-excess PMN-PT. *J. Am. Ceram. Soc.*, 2006, **89**(5), 1668–1672.
36. Kang, S.-J. L., *Sintering: Densification, Grain Growth & Microstructure*. Elsevier, Amsterdam, 2005, pp. 145–162.
37. Li, J. F., Zhen, Y., Zhang, B. P., Zhang, L. M. and Wang, K., Normal sintering of (K, Na)NbO_3-based lead-free piezoelectric ceramics. *Ceram. Int.*, 2008, **34**, 783–786.
38. Shigemi, A. and Wada, T., Enthalpy of formation of various phases and formation energy of point defects in perovskite-type $NaNbO_3$ by first-principles calculation. *Jpn. J. Appl. Phys.*, 2004, **43**(9B), 6793–6798.
39. Shigemi, A. and Wada, T., Evaluations of phases and vacancy formation energies in $KNbO_3$ by first-principles calculation. *Jpn. J. Appl. Phys.*, 2005, **44**(11), 8048–8054.
40. Irle, E., Blachnik, R. and Gather, B., The phase diagrams of Na_2O and K_2O with Nb_2O_5 and the ternary system Nb_2O_5-Na_2O-Yb_2O_3. *Thermochim. Acta*, 1991, **179**, 157–169.
41. Fisher, J. G., Benčan, A., Godnjavec, J. and Kosec, M., Growth behaviour of potassium sodium niobate single crystals grown by solid-state crystal growth using $K_4CuNb_8O_{23}$ as a sintering aid. *J. Eur. Ceram. Soc.*, 2008, **28**, 1657–1663.
42. Yoon, B. K., Choi, S. Y., Yamamoto, T., Ikuhara, Y. and Kang, S.-J. L., Grain boundary mobility and grain growth behaviour in polycrystals with faceted wet and dry boundaries. *Acta Mat*er., 2009, doi:10.1016/j.actamat.2009.01.005.
43. Fisher, J. G., Choi, S. Y. and Kang, S.-J. L., Abnormal grain growth in barium titanate doped with alumina. *J. Am. Ceram. Soc.*, 2006, **89**(7), 2206–2212.
44. Park, Y. J., Hwang, N. M. and Yoon, D. Y., Abnormal growth of faceted (WC) grains in a (Co) liquid matrix. *Metal. Mater. Trans. A*, 1996, **27A**, 2809–2819.